Biochimica et Biophysica Acta 1838 (2014) 1191–1198

Contents lists available at ScienceDirect

Biochimica et Biophysica Acta

journal homepage: www.elsevier.com/locate/bbamem

Quantitative analysis of individual hepatocyte growth factor receptor clusters in influenza A virus infected human epithelial cells using localization microscopy ☆

Qiaoyun Wang [a,f], Rüdiger Dierkes [b], Rainer Kaufmann [a,c,d], Christoph Cremer [a,e,f,*]

[a] Kirchhoff Institute for Physics, University of Heidelberg, D-69120 Heidelberg, Germany
[b] Institute of Molecular Virology, University of Münster, D-48149 Münster, Germany
[c] Division of Structural Biology, Wellcome Trust Centre for Human Genetics, Oxford, United Kingdom
[d] Department of Biochemistry, University of Oxford, Oxford, United Kingdom
[e] Superresolution Light Microscopy, Institute of Molecular Biology (IMB), Mainz, Germany
[f] Institute of Pharmacy and Molecular Biotechnology, University of Heidelberg, D-69120 Heidelberg, Germany

ARTICLE INFO

Article history:
Received 15 July 2013
Received in revised form 26 November 2013
Accepted 20 December 2013
Available online 27 December 2013

Keywords:
Superresolution/Localization microscopy
nanoscopy
Influenza viruses
Hepatocyte growth factor receptor
Single molecules
SPDM
SMLM
SALM

ABSTRACT

In this report, we applied a special localization microscopy technique (Spectral Precision Distance/Spatial Position Determination Microscopy/SPDM) to quantitatively analyze the effect of influenza A virus (IAV) infection on the spatial distribution of individual HGFR (Hepatocyte Growth Factor Receptor) proteins on the membrane of human epithelial cells at the single molecule resolution level. We applied this SPDM method to Alexa 488 labeled HGFR proteins with two different ligands. The ligands were either HGF (Hepatocyte Growth Factor), or IAV. In addition, the HGFR distribution in a control group of mock-incubated cells without any ligands was investigated. The spatial distribution of 1×10^6 individual HGFR proteins localized in large regions of interest on membranes of 240 cells was quantitatively analyzed and found to be highly non-random. Between 21% and 24% of the HGFR molecules were located in 44,304 small clusters with an average diameter of 54 nm. The mean density of HGFR molecule signals per individual cluster was very similar in control cells, in cells with ligand only, and in IAV infected cells, independent of the incubation time. From the density of HGFR molecule signals in the clusters and the diameter of the clusters, the number of HGFR molecule signals per cluster was estimated to be in the range between 4 and 11 (means 5–6). This suggests that the membrane bound HGFR clusters form small molecular complexes with a maximum diameter of few tens of nm, composed of a relatively low number of HGFR molecules. This article is part of a Special Issue entitled: Viral Membrane Proteins — Channels for Cellular Networking.

1. Introduction

Influenza A (IAV) is capable of rapid-genetic changes in mammals. It is an important pathogen that causes acute diseases of the respiratory tract in millions of people each year all over the world. The IAV subtype H1N1 is currently endemic in both human and pig populations [56,58]. Previous studies [21] have presented first indications of an interplay of IAV with receptor tyrosine kinases (RTKs). If so, RTKs would be expected to possibly play a role in the mechanism of IAV entry into the cells. Furthermore, RTKs have been shown to exert a critical role in the development and progression of many types of cancer [65]; hence a direct binding of IAVs to RTK complexes, or some indirect mode of affecting their structure, composition or spatial distribution on the membrane might also affect cellular processes correlated with cancer. It is hence of great importance to study in as much detail as possible the effects of IAV on specific RTK receptor molecules on the cell membrane and the influence on their expression and distribution. This makes it highly desirable to complement presently used bulk methods (such as immunoprecipitation, Western-blotting) with analyses on the single molecule resolution level. In contrast to bulk analyses typically averaging thousands or millions of cells, such enhanced resolution techniques would allow to study in individual cells the influence of IAV on the spatial distribution of single cancer related cellular signaling receptor molecules. However, due to their limited optical resolution (about 200 nm in the object plane), conventional immunofluorescence microscopy approaches are not sufficient to achieve this goal.

In this report, we used super-resolution fluorescence microscopy to study on the single cell/single molecule level a possible relationship between IAV infection and changes in the spatial distribution of the membrane based Hepatocyte Growth Factor Receptor (HGFR) in human alveolar basal epithelial cells.

☆ This article is part of a Special Issue entitled: Viral Membrane Proteins — Channels for Cellular Networking.

* Corresponding author at: Kirchhoff Institute for Physics, University Heidelberg, D-69120 Heidelberg, Germany. Tel.: +49 6131 39 21518.
E-mail addresses: c.cremer@imb-mainz.de, cremer@kip.uni-heidelberg.de (C. Cremer).

0005-2736/$ – see front matter © 2013 Elsevier B.V. All rights reserved.
http://dx.doi.org/10.1016/j.bbamem.2013.12.014

HGFR [14,25] is a protein encoded by *c-met* that is a proto-oncogene related to process tyrosine-kinase activity [15]. HGF is the only known ligand of the HGFR. The HGF receptor (HGFR) is a major regulator of proliferation, migration, and survival for many epithelial cell types. Via its binding, HGF transduces multiple biological effects such as mitogenesis, motogenesis, metastogenesis and morphogenesis [14,63].

In the last two decades, new developments in photophysics and optical technology have made it possible to establish various far field fluorescence microscopy techniques by which the conventional light optical resolution limits [1,48] of about 200 nm (object plane) have been substantially overcome.

This progress was achieved by using optical conditions not subject to the conditions of the Abbe/Rayleigh theories [for reviews see [16,17,32,33]]. Due to these developments of "superresolution"/"nanoscopy" techniques of far field light microscopy, the distribution of membrane proteins can now be studied at substantially enhanced resolution, using fluorescence microscopy with a resolution down to the molecular level. For example, stimulated emission depletion microscopy (STED) based on a scanning approach revealed that the membrane protein syntaxin formed protein clusters with a diameter of 50 to 60 nm [54]. Another "superresolution" or "nanoscopy" approach denoted as Patterned Excitation or Structured Illumination microscopy (PEM/SIM) [7,27,31] achieved an optical resolution (object plane) in the 100 nm range by using a structured pattern of the light distribution in the object plane instead of the conventional homogeneous illumination; axially structured illumination methods allowed the measurement of the extent of small fluorescent labeled structures along the optical axis down to sizes in the few tens of nm range [2–4,7,40,49].

In addition to scanning and structured/patterned illumination based nanoscopy approaches, methods of spectrally assigned localization microscopy (SALM) techniques are becoming more and more used to study cellular nanostructures. Generally, these techniques are based on the independent registration of the diffraction images ("optical isolation") produced by point emitters using appropriate differences in their spectral signatures [10,13,18,20,28]. For example, differences in the time dependent absorption/emission spectrum [61]; the fluorescence emission spectrum [22,23,47]; the fluorescence life time [29]; or the time dependent stochastic switching of fluorescence emission characteristics [9,11,12,24,30,34,37,42,44,49,50,57] have been used for the optical isolation of the diffraction images of the point emitters. In this way it became possible to assign the center/maximum of the diffraction images independently from each other, the center coordinates thus determined being correlated with the position of the point emitter in the object plane; consequently, positions and hence distances between point emitters can be determined independently from each other, and thus the conventional resolution limit can be overcome. Recently, SALM methods for stochastic photoswitching of fluorescence emission spectra such as Photo Activated Localization Microscopy (PALM) [11], Stochastic Optical Reconstruction Microscopy (STORM) [50], Fluorescence Photo Activated Localization Microscopy (FPALM) [34], PALM with Independently Running Acquisition (PALMIRA) [12], Spectral Precision Distance/Position Determination Microscopy with Physically modified fluorochrome (SPDM*Phymod*) [42,43,49], direct STORM (dSTORM) [30,57] and various related approaches [5–8] have made it possible to image cellular nanostructures down to the single molecule resolution level [for reviews see [17,19,36,60,64]]. A special feature of the SPDMPhymod technique applied here (in the following abbreviated as SPDM) is the use of conventional green fluorescent proteins/fluorophors and standard preparation conditions, together with photoswitching/readout by a single laser frequency for a given molecule type [26,39,42,43,49]. This SPDM variant based on reversible photoswitching [55] has already been successfully applied in a number of membrane protein studies, such as the analysis of breast cancer related Her2/neu clusters [40]; the analysis of claudin networks [41]; or the analysis of glycoproteins in a cellular blood–brain interaction model [38]. Here, we report for the first time the use of localization microscopy/SPDM to analyze down to the individual cell/single molecule resolution level the influence of influenza IAV infection on the spatial distribution of HGFR membrane proteins.

From a general perspective, this approach provides the methodological basis to analyze also other kinds of virus–cell interactions at single molecule resolution level in individual, intact and eventually live cells; furthermore, it opens an avenue to study on the single cell level the interaction of individual drug molecules to influence virus-receptor interactions.

2. Material and methods

2.1. Cell culture, sample preparation, immunofluorescence staining

The human lung epithelial cell line A549 was cultivated in DMEM (PAA) supplemented with 10% heat-inactivated fetal bovine serum (FCS, Biochrom). Conventional object slides were used. One day prior to infection, cells were seeded on cover slides at 80% of confluency. Three different treatments were applied: For negative control (treatment I), the cells were incubated with Opti-MEM (mock infected). For IAV infection (treatment II), the cells were inoculated with influenza virus A/Puerto Rico/8/34 (H1N1). To allow the IAV particles to attach, the cells were incubated at 4 °C for 1 h after addition of the inoculum. For positive control (treatment III), cells were treated with recombinant human HGF (R&D Systems) at a concentration of 30 ng/ml (in Opti-MEM). The inoculum of the negative controls (mock infected, treatment I) just contained medium (Opti MEM + Glutamax, Invitrogen); the positive controls (treatment III) contained medium and HGF (final concentration 30 ng/ml) and the inoculum of IAV treated cells (treatment II) contained medium and virus particles at a multiplicity of infection (MOI) of 100 (this means on average 100 infectious particles per cell). Thereafter, all cells (treatments I–III) were incubated at 37 °C in a standard CO_2 incubator for the times indicated (5, 10, 15 and 30 min) before they were fixed on the cover slip and stained. For this, the inoculum was removed; cells were washed twice with PBS and fixed with formaldehyde (Roth, 3.7% v/v in PBS) at room temperature (RT) for 20 min. For permeabilization, cells were then incubated with 0.2% (v/v) Triton X 100 at RT for 2 min. Cells were washed two times with PBS, before rabbit anti-HGFR polyclonal antibody was added (Santa Cruz, 1:100 in PBS containing 10% (v/v) FCS). After an antibody incubation time of 30 min, cells were washed three times with PBS, and Alexa488 labeled goat anti-rabbit antibodies were added for another 30 min (Invitrogen, 1:300 in PBS containing 10% (v/v) FCS). Afterwards, cells were washed five times with PBS followed by a wash with ddH_2O; embedding was carried out with Prolong Gold antifade reagent (Invitrogen, Carlsbad, CA, USA), and the coverslip was sealed with nail polish.

2.2. SPDM setup

For localization microscopy, a variant of spectral precision distance/position determination microscopy (SPDM) [13,18–20] was used which allowed photoswitching of conventional fluorochromes using conventional specimen preparation conditions in combination with a single laser wavelength of appropriate illumination intensity both for excitation and registration, as reported previously [39–43].

The SPDM setup used has been described in detail [16,26,39,42]. Briefly, a diode pumped solid-state (DPSS) laser with a wavelength of 488 nm (Sapphire HP488, Coherent, Dieburg, Germany) was utilized for exciting fluorescent antibody bound Alexa 488 molecules. The specimens were illuminated by the defocused laser beam (object plane diameter several tens of μm) using a high aperture objective lens (63×/NA1.4.oil). The fluorescent light excited was transmitted through a dichroic mirror and an emission filter and then imaged via a lens with a magnification of 1.0× onto a highly sensitive CCD-camera.

To obtain a SPDM image with enhanced resolution, typically 1000 frames of the same field of view of the same object were taken at a

frame rate of 10/s, using an illumination intensity of about 25 kW/cm^2. By fitting a two dimensional Gaussian with a linear estimation of the background noise to single molecule signals, the positions of the registered molecule signals were determined (for details see [39]). All the positions found were assigned to a single localization map.

For visualization of the position data in the localization map, various image representations were generated [39–41]. By blurring the position of each individual molecule signal corresponding to the individual localization accuracy, an image was obtained which corresponded to the actually achieved optical resolution: Two adjacent, blurred molecule signals in a distance dmin still separated from each other indicated a similar (two-point) optical resolution valid for fluorescent point emitters according to the Rayleigh criterium [48]. To obtain a visualization of the structural resolution achieved [17], the localization map was rendered by the density of the detected molecules and the localization accuracy [41]. In the experiments reported here, the mean estimated localization accuracy was 29 nm (standard deviation). While the density rendered image facilitates the visual inspection of structural details, the unblurred localization map makes possible detailed quantitative analyses, such as counting of individual molecule signals, distance frequency distributions etc. In this report, all analyses and conclusions were based on the direct evaluation of the original localization map, taking into account the limits in (optical and structural) resolution obtained.

2.3. Data analysis

Using the SPDM method outlined above, localization maps of the positions of single HGFR molecules were obtained. This allowed the analysis of the spatial distribution of HGFR proteins as a function of the incubation time (treatment I:mock infection = control; treatment II: IAV infection; treatment III:HGF binding). From the localization map, normalized frequencies were calculated for the distance distribution of the HGFR molecules on the membrane; in addition, simulated distance distributions of randomly localized signals [26] were obtained and normalized in the same way as the experimental HGFR locations.

To identify aggregations of HGFR molecules, a local density based cluster definition was used [40]: a cluster was defined as an ensemble of molecules where around each molecule signal, three or more neighboring signals were counted within the radius of 60 nm. This means that all molecules detected in a cluster had at least three neighbors detected within a distance of 60 nm. Since each of these molecules has at least 3 neighbors, the minimum total number of molecules detected in a cluster was 4. This definition allows clusters that are either smaller in size (e.g. a total of 4 molecules with a maximum of mutual distances of 30 nm, corresponding to a diameter of e.g. 30 nm only); or clusters which have a size much larger than an area of radius r = 60 nm (e.g. 10 molecules within a circular area of diameter 2r = 150 nm, where each of the 10 molecules has at least 3 neighbors within a distance of 60 nm). Hence, the cluster algorithm used can identify very small clusters (e.g. 30 nm Ø) with a very low number of molecule signals (e.g. $N_{CL} = 4$), as well as large clusters (e.g. 150 nm Ø, with a high number of molecule signals, e.g. $N_{CL} = 20$). For comparison, random distributions of points were generated with the same mean density as the localization data. For further details, see [40].

3. Results

For the SPDM imaging of A549 cells, Alexa488 was used for indirect immunolabeling of HGFR membrane proteins. All SPDM measurements were performed at an excitation wavelength of 488 nm for both photoswitching and fluorescence registration. In total, the spatial distribution of about 1 million individual HGFR molecule signals was analyzed on the membrane of 240 different cells, using four different incubation times (5 min, 10 min, 15 min, 30 min) and three different treatments: Mock incubation/control (no HGF ligand, no IAV); incubation with the HGF ligand alone; and incubation with the IAV alone. In each of the 240 cells analyzed, a large region of interest (typically in the order of 20 × 20 μm^2) was illuminated in the SPDM mode described above. In this report, all the data presented refer to these regions of interest (ROI), i.e. to the results obtained for 240 ROIs in 240 different cells. To eliminate a bias due to possible variations in the size of the SPDM illuminated ROIs and their positions inside the cells, all the conclusions drawn were done in such a way that such variations do not play a role. From the average SPDM localization accuracy σloc = 29 nm (standard deviation) achieved in these experiments, an average (two-point) single molecule optical resolution of about 60 nm may be inferred [39].

3.1. Visual inspection of SPDM images reveals HGFR nanostructures far below the conventional resolution limit

Fig. 1 shows conventional wide-field images (Fig. 1A–C) and high resolution (SPDM) images of a ROI in an IAV infected cell after an incubation time of 5 min (Fig. 1D–F). Already from the conventional resolution images (1A–C), it is obvious that the spatial distribution of the HGFR proteins on the cell membrane is very heterogeneous; obviously, many of them are arranged in small clusters. The conventional resolution enlargements in Fig. 1B, C suggest that these clusters might be even as large as several hundred nm in diameter, corresponding to the optical resolution limit. This means, however, that these HGFR clusters might also be much smaller than the ca. 200 nm apparent in the conventional resolution image (compare Fig. 1C). Therefore it is impossible to obtain a more correct estimate of the size of the HGFR clusters from these conventional resolution images (Fig. 1A–C). Such a more correct estimate, however, became possible using localization microscopy (SPDM). On the right side of Fig. 1, such SPDM images (Fig. 1D–F) are shown for the corresponding conventional resolution regions see Fig. 1A–C). The visual inspection confirms the highly heterogeneous distribution of the HGFR clusters already visible in the conventional resolution images. Due to their superior optical resolution, however, the SPDM images indicate that a) the number of clusters is much larger than detected in the conventional resolution images; and b) that the size of the clusters is in reality much smaller (below 100 nm).

The visual inspection of such SPDM images has a number of setbacks: While it indicates a large number of HGFR clusters of an apparent size below 100 nm, so far it provides no quantitative information (as a function of the treatment of the cells) on a) the average size (diameter) of the clusters; b) the number/density of the clusters; c) the spatial distribution of the clusters on the cell membrane; d) the number/density of HGFR molecules inside and outside such clusters; and e) the number of HGFR molecules/cluster.

3.2. The distribution of individual HGFR molecules on the membrane is highly non-random

The visual inspection of the SPDM images suggested that the HGFR molecules form small clusters distributed all over the membrane. In case this assumption is correct, one would expect a strong deviation of the single molecule positions from a random spatial distribution. To test and quantify the hypothesis of a highly heterogeneous spatial distribution of the HGFR molecules on the cell membrane, normalized frequency distance distributions were calculated for all HGFR molecule signals detected. Fig. 2 shows the result using the HGFR localization data obtained by SPDM from all the 240 ROIs in the 240 cells measured (total of 1,027,944 molecule positions). In this graph, for each of the ca. 1 million positions the distances to all other molecules detected on the membrane of a given cell within a radius of 200 nm were determined; the frequency of occurrence of a certain distance was normalized to the total number of all detected signals as previously described [40]. For all treatments (mock-incubation/normal; incubation with HGF ligand; and incubation with IAV), a broad distance distribution was observed. The distance distribution for the IAV infected cells, however,

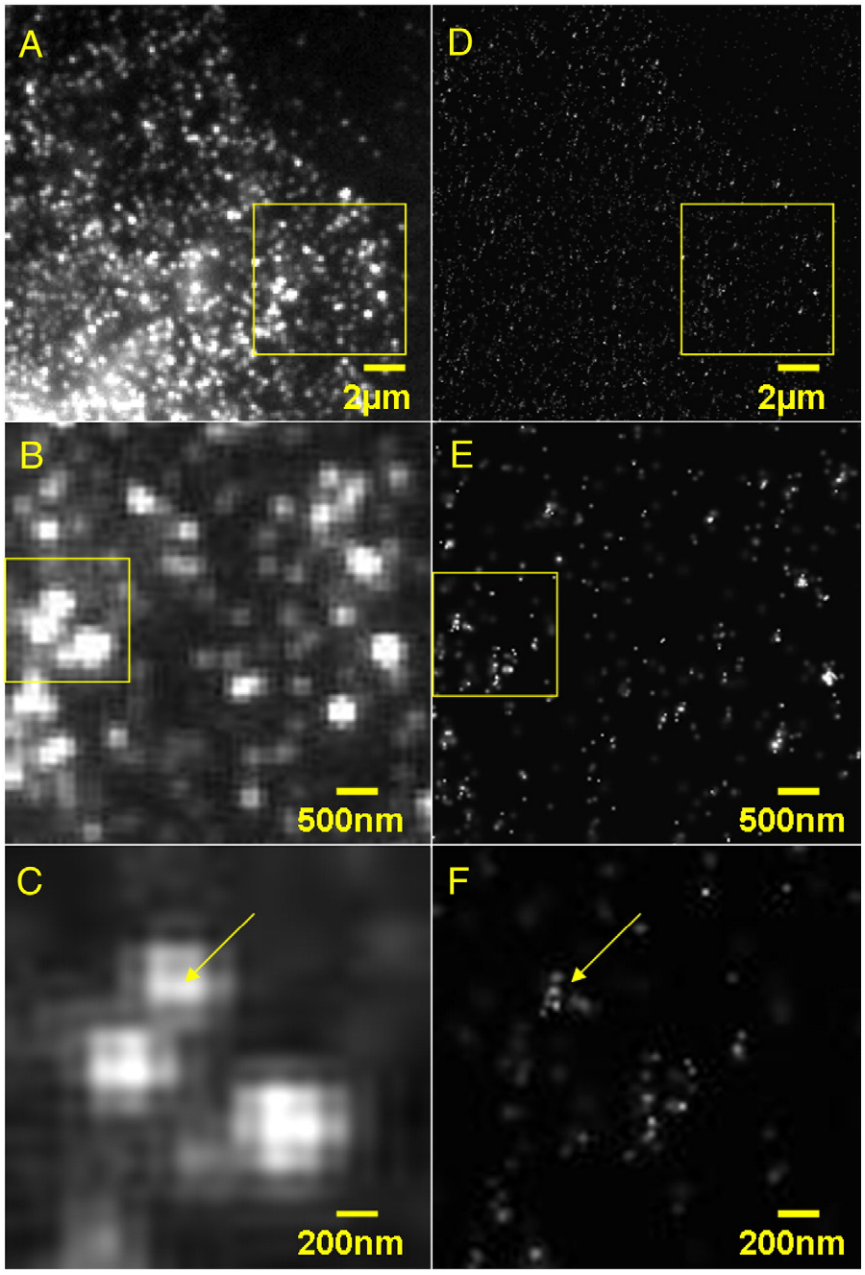

Fig. 1. Images of Alexa 488 immunolabeled HGFR protein clusters on the membrane of A549 cells after 5 min incubation time. (A)–(C) Conventional wide field fluorescence (conventional resolution). (A) Overview, part of an A549 cell membrane. The ROI is about 20 × 20 μm^2. (B) Enlarged conventional resolution image of the rectangular insert box in image A; (C) enlargement of the conventional resolution image (B). (D)–(F) Localization microscopy (SPDM) images of the corresponding cellular regions. (D) SPDM image corresponding to area (A). (E) SPDM image corresponding to area (B). (F) SPDM image corresponding to area (C). All SPDM images were obtained after blurring of the individual HGFR localization maps with a Gaussian with standard deviation of 29 nm, corresponding to the average localization accuracy achieved. Scale bars are increased from 2 μm (A, D) to 500 nm (B, E) to 200 nm (C, F).

shows a clear maximum around 40 nm distance, while the HGF treated cells (ligand) and the mock treated control cells indicated a clear shoulder at this value. To decide whether this distributions deviate from a random distribution, a normalized distance frequency distribution was calculated in the same way, as previously described [40]; this time, however, in these numerical simulations the molecule positions were assumed to be randomly distributed over the cell membrane. The normalization of all frequency data was done in such a way that the simulated random distribution resulted in a linear increase of frequency with the molecule–molecule distances. As Fig. 2 shows, a very pronounced difference was obtained between the experimental distance distributions and the simulated random distributions. We conclude that the overall distribution of the HGFR molecules over the cell membrane was highly heterogeneous.

3.3. The HGFR clusters have an average diameter in the 50 nm range

The quantitative distance frequency results shown in Fig. 2 clearly indicated a highly heterogeneous distribution of the individual HGFR molecules, suggesting the existence of HGFR clusters. Therefore, the next step was to identify such clusters, to count their number and density, and to determine their size. As the visual inspection (Fig. 1) indicated, these clusters have a size substantially smaller than the conventional resolution limit of about 200 nm: In the enhanced resolution SPDM image, one of the HGFR "spots" seen in the conventional microscopy image (Fig. 1B,C) may be composed of numerous small HGFR clusters, each with a size considerably smaller than 100 nm (Fig. 2E,F).

Using the density based algorithm for cluster size determination previously described to analyze Her2/neu clusters in breast cancer

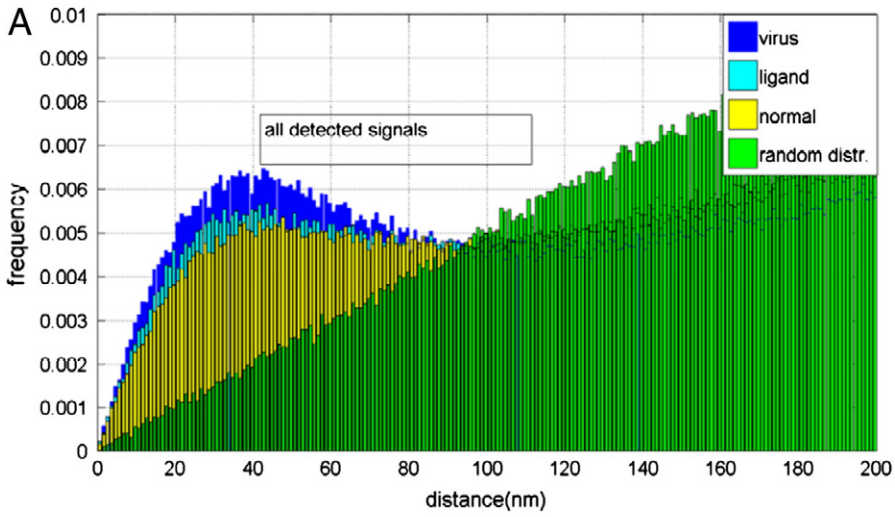

Fig. 2. Quantitative SPDM analysis of the overall spatial distribution of HGFR signals on the cell membrane. Ordinate: normalized frequency of the occurrence of specific molecule–molecule distances, for mock incubated control cells (yellow); HGF ligand incubated cells (light blue); for IAV incubated cells (dark blue); and for a simulated random molecule distribution (green). For the calculations, all HGFR positions detected on the membrane of a given cell were considered. Abscissa: distance from a given HGFR signal to a neighboring molecule within a radius of 200 nm. For each HGFR position detected, all distances up to 200 nm were determined. The experimental distance frequency distributions were based on SPDM data from a total of 240 cells (80 control cells, 80 ligand treated cells, 80 IAV infected cells) with a total of 1 million molecule positions. In each category, the distance frequencies for the different incubation times (5, 10, 15, 30 min) were pooled.

cells [40], for each cluster (containing at least 4 individual HGFR molecule signals with mutual distances ≤ 60 nm) the diameter dcluster was determined. The values obtained varied from about 20 nm up to about 120 nm (Fig. 3). A clear peak, however, was obtained around 40–50 nm. Altogether, the average apparent cluster diameter was dcluster = 54 nm ± 24 nm (standard deviation, SD) and independent of the treatment of the cells (data not shown). This figure is about 4 times smaller than suggested by conventional resolution microscopy (compare Fig. 1B, C). Since the (two point) optical resolution achieved in the SPDM imaging reported here was on average in the order of 2 × σloc ~ 60 nm [39], the true HGFR cluster diameter might even be somewhat smaller than 54 nm. Diameters much higher than this value observed at relatively low frequencies might be explained by a vicinity of several ~Ø 50 nm clusters too close to be distinguished by the algorithm. The validity of such an interpretation may be justified from the visual inspection of the SPDM images (see Fig. 1F) where a number of small clusters (Ø smaller 100 nm) was observed to be close to each other.

3.4. In IAV infected cells, the HGFR clusters contain a substantial percentage of all the HGFR proteins on the cell membrane

The next question we asked was: How many HGFR molecules are within the clusters identified, compared to the HGFR molecules outside of these clusters? To answer this, it was first necessary to identify in all the ROIs the clusters with appropriate resolution, and next to count the number of HGFR molecule signals within and outside of these clusters. This became possible only using a technique of single molecule based localization microscopy, like SPDM. The results obtained from the SPDM based position maps are summarized in Table 1. To allow a direct comparison, the numbers refer to the total no. of HGFR molecule signals within given ROIs and the no. N_{CL} of HGFR molecule signals within the clusters in the same ROIs.

As Table 1 shows, there is a certain variation of the percentage of HGFR molecules within the clusters, ranging from a minimum of 14% to a maximum of 29%. On average, however, there appears to be at best a slight increase only between mock treated control cells and IAV

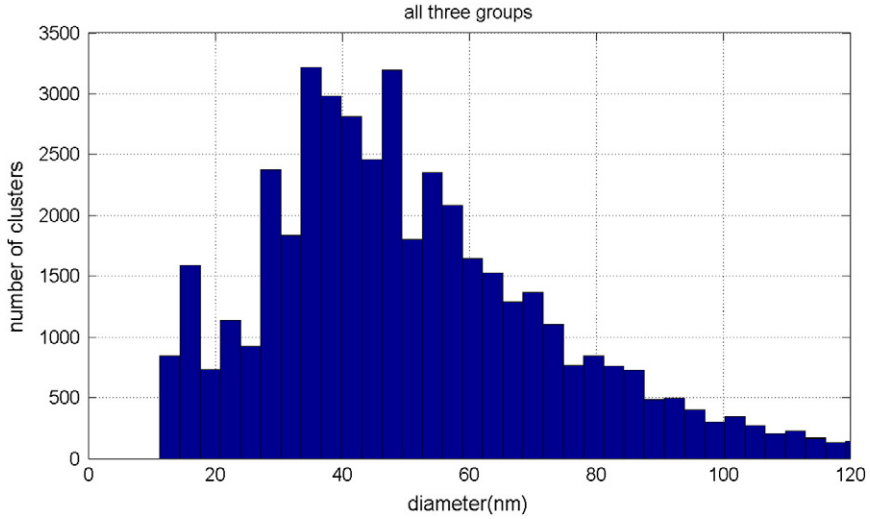

Fig. 3. Frequency distribution of HGFR cluster size. Ordinate: number of clusters with a given diameter (in a total of 240 ROIs in 240 cells). Abscissa: diameter of HGFR cluster as determined by a density based algorithm ([40]; see Material & methods section). Total no. of clusters evaluated: 44,304.

Table 1
Distribution of HGFR molecule signals within and outside of the clusters.

Incubation time [min]	Control		HFG-ligand		IAV infection	
	Total no. HGFR molecule signals/ROI	No. HGFR molecules in the clusters/ROI	Total no. HGFR molecules/ROI	No. HGFR molecules in clusters/ROI	Total no. HGFR molecules/ROI	No. HGFR molecules in clusters/ROI
5	82,023	18,865 (23%)	71,268	14,254 (20%)	92,060	26,697 (29%)
10	89,747	21,539 (24%)	87,641	22,787 (26%)	99,077	22,788 (23%)
15	72,472	14,494 (20%)	81,049	20,262 (25%)	103,953	19,751 (19%)
30	66,885	9364 (14%)	91,334	16,440 (18%)	90,435	24,417 (27%)
Sum (total molecule number for each group of treatment) (80 cells)	311,127	64,263 (21%)	331,292	73,743 (22%)	385,525	93,653 (24%)

infected cells; altogether, on average the percentage of HGFR molecules within the clusters as compared to the HGFR molecules detected outside the clusters in the same cells varies by a few percent (between 21% and 24%) only. In contrast, the total absolute no. of HGFR molecule signals detected varied somewhat more (from 311,127molecules/80 = 3889 molecules/cell for mock treated control cells) to 385,525molecules/80 = 4819 molecules/cell for IAV infected cells, corresponding to an increase of 24%.

3.5. The HGFR clusters are composed of a relatively small number of protein molecules

So far, a considerable variation was observed of the total number of HGFR molecules detected per cell, as well as of the total number of HGFR clusters expressed per cell. Is this variability found also for the number of HGFR molecules per cluster? Can we make an estimate of the number of molecules in an individual cluster?

As a first step to obtain this figure, for each condition (treatment, incubation time), the mean molecule density in the clusters was determined automatically as described [40]. The result is shown in Table 2. For each condition and incubation time, 20 cells were measured (total 240 cells).

Surprisingly, in contrast to the considerable variations of the absolute numbers of HGFR proteins detected in the individual experiments, the detected HGFR protein densities in the clusters turned out to be quite stable: The overall variation in the density values for different treatments and incubation times was around 10% only; in the individual groups, the standard deviation in the protein density was around 5%–7% only.

Using the average diameter obtained from the density related algorithm for the HGFR clusters (54 nm), a first estimate may be obtained for the number of HGFR molecules detected in an individual cluster: Assuming an average circular diameter of the HGFR clusters of 54 nm, and 2194 HGFR molecule signals in 1 μm^2 (control cells), a cluster area of Acl = $\pi \times [54 \times 10^{-3}\ \mu m/2]^2 = 2.3 \times 10^{-3}\ \mu m^2$ and hence a number Ncl of HGFR protein signals/cluster of N_{CL} (control) = 2194 × Acl = 5.02 HGFR molecule signals/cluster was obtained; for cells incubated with the HGF ligand, the corresponding figure was NCL (HGF) = $2187 \times 2.3\ 10^{-3}\ \mu m^2$ = 5,0 HGFR molecule signals/cluster; for IAV incubated cells NCL (PR8) = $2463 \times 2.3\ 10^{-3}$ µm2 = 5.7 molecule signals/cluster was obtained. Taking into account the variability of the cluster sizes determined (Fig. 3; dcluster = 54 nm ± 24 nm), in the same way as above one, values between 2 molecule signals per cluster (for dcluster = 54 nm–24 nm) and 11 molecules per cluster (for $d_{cluster}$ = 54 nm + 24 nm) are calculated. Since the minimum number of signals per cluster was algorithmically defined to be 4, this lower value is too small by definition; from this, on average the number of HGFR molecule signals per cluster is estimated to range between 4 and 11.

Table 2
Molecule signal density in HGFR clusters per μm^2. For each condition and incubation time, 20 cells were measured (total 240 cells).

Incubation time	Control cells ($1/\mu m^2$)	HGF ligand ($1/\mu m^2$)	IAV infection ($1/\mu m^2$)
5 min	2275.3	2262.4	2507.1
10	2258.1	1969.3	2599.7
15	2220.2	2101.5	2214.3
30	2022.1	2413.8	2529.8
Mean molecule signal density in cluster (+/− SD)	**2194 ± 101**	**2187 ± 167**	**2463 ± 166**

4. Discussion

Recently, receptor tyrosine kinases (RTKs) were shown to be engaged as cellular signaling receptors during the entry of influenza A viruses (IAV) into the cells [21]. In particular, siRNA-mediated knock down of HGFR resulted in impaired IAV uptake, indicating a correlation between the HGFR receptor and IAV entry [21]. Such a correlation might be due to e.g. direct effects (binding of IAV to HGFR), or indirect effects (binding of IAV to another receptor which in turn is affected by the presence of HGFR [59,62]). In both cases, the spatial distribution of HGFR on the membrane might play a role for the IAV uptake. Inversely, IAV infection might affect the intracellular distribution of HGFR and thus possibly exert some influence on HGFR related effects. To test such a hypothesis, we investigated in this report for the first time a possible connection between IAV infection and HGFR distribution on the single molecule/single cell level using spectral precision distance/spatial position determination microscopy (SPDM), a method of super-resolving spectrally assigned localization microscopy (SALM). Such methods have already been shown to be particularly useful to study the spatial distribution of individually resolved membrane based molecules at the nanometer resolution scale [6,11,34–36,38,41,52,53]. For example, using the special SPDM technique applied here, it became possible to study quantitatively at the molecular resolution level the spatial distribution of Her2/neu receptor clusters [40].

The application of localization microscopy (SPDM) to the analysis of HGFR receptor proteins reported here showed that IAV infection was correlated with changes on the nanoscale: the visual inspection of the 'nanoscopic' images revealed HGFR nanostructures far below the conventional resolution limit; the amount of membrane associated HGFR proteins (as estimated from the number of HGFR signals in the ROIs of the single cells) appeared to be somewhat increased in IAV infected cells; the distribution of individual HGFR molecules at the membrane was highly non-random; the individual HGFR clusters (defined to contain at least 4 HGFR molecule signals within mutual distances not larger than 60 nm) were determined to have an average diameter in the 50 nm range; in IAV infected cells, the HGFR cluster density was

increased and the HGFR clusters contained up to almost 30% of all the HGFR molecule signals localized in the ROIs. Since these regions of interests covered large parts of the entire cellular areas, these percentages will probably be valid for the entire cell membranes. Furthermore, in the same ROI, one may expect that the photoswitching conditions allowing optical isolation have been similar for HGFR proteins within and out of the clusters; hence, the percentages may be valid also for the HGFR molecules themselves.

It is interesting to note that both the total number of membrane associated HGFR molecule signals/ROI and the number of the HGFR molecules in the clusters/ROI were dependent on the time of incubation (Table 1): For example, if one compares short incubation times (5 min) with longer incubation times (30 min), the control cells showed a marked decrease with time (from ca. 82,000 total number to ca. 67,000); on the contrary, the HGF-ligand incubated cells indicated an increase (from ca. 71,000 total number to 91,000); while the IAV infected cells suggested first a rise of total membrane associated HGFR numbers with incubation time (from 92,000 at 5 min incubation time to ca. 104,000 at 15 min, followed by a decrease at 30 min). To what extent these (altogether relatively small) temporal changes reflect methodological problems of the present SPDM method (e.g. slight variations in the effective illumination intensity, or in the composition of the "photoswitching" medium), or indicate real changes in the cellular distribution of HGFR receptors, remains to be investigated.

A major result of these SPDM analysis was the discovery that individual HGFR clusters may be composed of a relatively small number N_{CL} of proteins. Combining the experimental results for the density ρ_{CL} of HGFR signals in the clusters with the cluster size $Ø_{CL}$, estimates for N_{CL} between 4 and 11 signals per cluster were obtained. For these calculations, the HGFR density values ($\rho_{CL} = N_{CL} / A_{CL}$) of the clusters (automatically determined by the cluster density algorithm) were multiplied with the area of the clusters (determined from the cluster diameter $Ø_{CL}$ automatically obtained from the cluster sizing algorithm). Interestingly, on average a number of HGFR protein signals/cluster $N_{cl} = 5.0$ HGFR molecule signals/cluster was estimated for control cells (mock incubation, treatment I); for cells incubated with the HGF ligand (treatment III), the corresponding figure was again $N_{CL} = 5{,}0$ HGFR molecule signals/cluster; for IAV infected cells (treatment II), however, a somewhat higher value $N_{CL} = 5.7$ molecule signals/cluster was obtained. It is tempting to speculate that such a result may be interpreted to suggest a direct or indirect influence of the IAV on the HGFR clusters in such a way that the number of HGFR molecules in the clusters was increased, or that the size of the HGFR cluster was slightly altered. Such an effect might be explained to be due either to a direct binding mechanism, or due to a binding to another receptor which in turn would act upon the HGFR receptor. To substantiate or refute such a hypothesis is beyond the scope of this paper. From the methodological point of view, however, it should be possible to test a direct binding of individual IAVs to individual HGFR clusters by dual color localization microscopy [8,19,26]: In this case, one would label the IAV coat proteins using a fluorphore A (e.g. Alexa 568), and the HGF receptor proteins with a fluorphore B (e.g. Alexa 488, as in the present report). To exclude a possible adverse effect of fluorphore-labeled coat proteins on the IAV binding, it may be advantageous to use instead photoswitchable lipophilic dyes [51].

Since in the SPDM method used (as well as in other SALM approaches), the detection efficiency α (i.e. the number N_D of molecules detected/number N_L of molecules labeled) was found to be smaller than 1.0 [6,19,45], the number N_L of HGFR proteins labeled per cluster may be larger by a factor $1/\alpha$. Hence, the number N_{CL} of labeled HGFR molecules residing within the clusters might be up to several times larger than the number N_D detected. In case that the labeling efficiency β = [number N_L of labeled molecules] / [number N_{true} of molecules present] would also be known, even the "true" number (N_{true}) of protein molecules in the HGFR cluster (i.e. the number of molecules actually present) may be calculated ($N_{true} = N_D / [\alpha \times \beta]$). Since in these SPDM measurements, we were able to measure the number of detected molecules (N_D) only, at the present time a reliable estimate of the "true" number N_{true} cannot be given. We found, however, that in spite of substantial differences in the number of HGFR signals and clusters in the individual measurements, the signal density was similar in all the 12 different experiments (with a total of 240 cells with about 1 million HGFR signals and ca. 44,000 HGFR clusters evaluated); this suggests that under the conditions used, α and β may be regarded to be close to a constant value. Otherwise, one would have to assume very complex compensation mechanisms to explain the similar signal density values obtained.

To summarize, we conclude that a substantial part of the HGF-receptors present on the surface of the lung epithelial cells analyzed is organized in small clusters of HGFR proteins of a similar number (variation between 4 and 11 molecule signals).

For further investigations of the influence of IAV on individual HGFR cluster nanostructures, a substantially better localization accuracy would be needed than the average of 29 nm achieved in these experiments. From the optical point of view, such an improved localization accuracy and hence optical resolution is indeed possible: e.g., using photoactivable Green Fluorescent Proteins (paGFP), localization accuracies in the 2 nm range have been reported for membranes in connection with background reduction by Total Internal Reflection (TIRF) Fluorescence microscopy [11]; with Alexa dyes, [45] successfully performed localization microscopy of individual nuclear pore complexes; using an atto dye coupled directly to coat proteins of individual tobacco mosaic virus (TMV) particles structures on a surface, at 488 nm excitation we obtained a SPDM localization accuracy down to the 2 nm scale, with an optical and structural resolution down to the 5 nm range [16,19]. Under very defined optical conditions, two Alexa molecules of the same type located on a glass surface have been reported to be resolved even at a distance of 1.3 nm, using visible light excitation for localization microscopy [46]. Numerical simulations [2] supported by proof-of-principle experiments [3] suggested that in combination with structured illumination/detection modes [4,49,53], a 3D resolution down to the 1 nm range should be possible from the point of Physics. Such a resolution would allow the unraveling of the three-dimensional structure of HGFR clusters and other biomolecular machines of the cell membrane to an extent which together with protein modeling would approach the level of resolution so far reserved to crystallography.

Acknowledgements

We gratefully acknowledge the support of Heidelberg University and of the Institute of Molecular Biology gGmbH. We thank very much Dr. Christina Ehrhardt, Institute of Molecular Virology, ZMBE University of Münster (Germany) for valuable advice and critical reading of the ms, as well as for the additional help obtained from colleagues in the Cremer Lab, in particular from Margund Bach, Gerrit Best, and Dr. Udo Birk.

References

[1] E. Abbe, Beiträge zur Theorie des Mikroskops und der mikroskopischen Wahrnehmung, M. Schultze's Arch. Mikrosk. Anat. IX (1873) 413–468.
[2] B.A. Albrecht, et al., Spatially modulated illumination microscopy: online visualization of intensity distribution and prediction of nanometer precision of axial distance measurements by computer simulations, J. Biomed. Opt. 6 (2001) 292–299.
[3] B.A. Albrecht, et al., Spatially modulated illumination microscopy allows axial distance resolution in the nanometer range, Appl. Opt. 41 (2002) 80–87.
[4] D. Baddeley, et al., Nanostructure analysis using spatially modulated illumination microscopy, Nat. Protoc. 2 (2007) 2640–2646.
[5] D. Baddeley, et al., Light-induced dark states of organic fluorochromes enable 30 nm resolution imaging in standard media, Biophys. J. 96 (2) (2009) L22–L24.
[6] D. Baddeley, et al., Optical single-channel resolution imaging of the ryanodine receptor distribution in rat cardiac myocytes, Proc. Natl. Acad. Sci. U. S. A. 106 (2009) 22275–22280.
[7] D. Baddeley, et al., Measurement of replication structures at the nanometer scale using super-resolution light microscopy, Nucleic Acids Res. 38 (e8) (2010) 1–11, http://dx.doi.org/10.1093/nar/gkp901.
[8] D. Baddeley, et al., 4D super-resolution microscopy with conventional fluorophores and single wavelength excitation in optically thick cells and tissues, PLoS ONE 6 (2011) e20645, http://dx.doi.org/10.1371/journal.pone.0020645.

[9] M. Bates, et al., Multicolor super-resolution imaging with photoswitchable fluorescent probes, Science 317 (2007) 1749–1753.
[10] E. Betzig, Proposed method for molecular optical imaging, Opt. Lett. 20 (3) (1995) 237–239.
[11] E. Betzig, et al., Imaging intracellular fluorescent proteins at nanometer resolution, Science 313 (2006) 1642–1645.
[12] H. Bock, et al., Two-color far-field fluorescence nanoscopy based on photoswitchable emitters, Appl. Phys. B 88 (2007) 161–165.
[13] H. Bornfleth, et al., High precision distance measurements and volumeconserving segmentation of objects near and below the resolution limit in three dimensional confocal fluorescence microscopy, J. Microsc. 189 (1998) 118–136.
[14] D.P. Bottaro, et al., Identification of the hepatocyte growth factor receptor as the c-met proto-oncogene product, Science 251 (1991) 802.
[15] C.S. Cooper, The met oncogene: from detection by transfection to transmembrane receptor for hepatocyte growth factor, Oncogene 7 (1992) 3–7.
[16] C. Cremer, Optics far beyond the diffraction limit from focused nanoscopy to spectrally assigned localization microscopy, in: F. Träger (Ed.), Springer Handbook of Lasers and Optics, 2nd edition, 2012, pp. 1351–1389.
[17] C. Cremer, B.R. Masters, Resolution enhancement techniques in microscopy, Eur. Phys. J. Hist. (EPJH) (2013), http://dx.doi.org/10.1140/epjh/e2012-20060-1.
[18] Cremer, C., et al. 1996. German Patent Application No. 196.54.824.1/DE, submitted Dec 23, 1996, European Patent EP 1997953660, 08.04.1999, Japanese Patent JP 1998528237, 23.06.1999, United States Patent US 09331644.
[19] C. Cremer, et al., Enhanced resolution imaging of biological nanostructures by spectral precision distance microscopy (SPDM), Biotechnol. J. 6 (2011) 1037–1051.
[20] C. Cremer, et al., Principles of spectral precision distance confocal microscopy for the analysis of molecular nuclear structure, in: B. Jähne, H. Haußecker, P. Geißler (Eds.), Handbook of Computer Vision and Applications, 3, 1999, pp. 839–857.
[21] Th. Eierhoff, et al., The epidermal growth factor receptor (EGFR) promotes uptake of influenza A viruses (IAV) into host cells, PLoS Pathog. 6 (e1001099) (2010) 1–16.
[22] A. Esa, et al., 3D-spectral precision distance microscopy (SPDM) of chromatin nanostructures after triple-colour labelling: a study of the BCR region on chromosome 22 and the Philadelphia chromosome, J. Microsc. 199 (2000) 96–105.
[23] A. Esa, et al., Conformational differences in the 3D-nanostructure of the immunoglobulin heavy-chain locus, a hotspot of chromosomal translocations in B lymphocytes, Cancer Genet. Cytogenet. 127 (2001) 168–173.
[24] J. Fölling, et al., Fluorescence nanoscopy by ground-state depletion and single-molecule return, Nat. Methods 5 (2008) 943–945.
[25] F. Galland, et al., Localization of the 5′ end of the MCF2 oncogene to human chromosome 15q15–q23, Cytogenet. Cell Genet. 60 (1992) 114–116.
[26] M. Gunkel, et al., Dual color localization microscopy of cellular nanostructures, Biotechnol. J. 4 (2009) 927–938.
[27] M.G.L. Gustafsson, Surpassing the lateral resolution limit by a factor of two using structured illumination microscopy, J. Microsc. 198 (2000) 82–87.
[28] T. Ha, et al., Dual-molecule spectroscopy: molecular rulers for the study of biological macromolecules, IEEE J. Sel. Top. Quantum Electron. 2 (1996) 1115–1128.
[29] M. Heilemann, et al., High-resolution colocalization of single dye molecules by fluorescence lifetime imaging microscopy, Anal. Chem. 74 (2002) 3511–3517.
[30] M. Heilemann, Subdiffraction-resolution fluorescence imaging with conventional fluorescent probes, Angew. Chem. 47 (2008) 6172–6176.
[31] R. Heintzmann, C. Cremer, Lateral modulated excitation microscopy: improvement of resolution by using a diffraction grating, Proc. SPIE 3568 (1999) 185–196.
[32] S.W. Hell, Far-field optical nanoscopy, Science 316 (2007) 1153–1158.
[33] S.W. Hell, Microscopy and its focal switch, Nat. Methods 6 (2009) 24–32.
[34] S. Hess, et al., Ultra-high resolution imaging by fluorescence photoactivation localization microscopy, Biophys. J. 91 (2006) 4258–4272.
[35] S.T. Hess, et al., Dynamic clustered distribution of hemagglutinin resolved at 40 nm in living cell membranes discriminates between raft theories, Proc. Natl. Acad. Sci. 104 (2007) 17370–17375.
[36] S.T. Hess, et al., Ultrahigh resolution imaging of biomolecules by fluorescence photoactivation localization microscopy, Methods Mol. Biol. 544 (2009) 483–522.
[37] B. Huang, et al., Three-dimensional super-resolution imaging by stochastic optical reconstruction microscopy, Science 319 (2008) 810–813.
[38] O. Huber, et al., Localization microscopy (SPDM) reveals clustered formations of P-glycoprotein in a human blood–brain barrier model, PLoS ONE 7 (e44776) (2012) 1–10.
[39] R. Kaufmann, et al., SPDM — single molecule superresolution of cellular nanostructures, Proc. SPIE 185 (2009)(71850J-1-71850-19).
[40] R. Kaufmann, et al., Analysis of Her2/neu membrane protein clusters in different types of breast cancer cells using localization microscopy, J. Microsc. 242 (2011) 46–54.
[41] R. Kaufmann, et al., Visualization and quantitative analysis of reconstituted tight junctions using localization microscopy, PLoS ONE 7 (2012) e31128.
[42] P. Lemmer, et al., SPDM: light microscopy with single-molecule resolution at the nanoscale, Appl. Phys. B Lasers Opt. 93 (2008) 1–12.
[43] P. Lemmer, et al., Using conventional fluorescent markers for farfield fluorescence localization nanoscopy allows resolution in the 10 nm range, J. Microsc. 235 (2009) 163–171.
[44] K.A. Lidke, et al., Superresolution by localization of quantum dots using blinking statistics, Opt. Express 13 (2005) 7052–7062.
[45] A. Löschberger, et al., Super-resolution imaging visualizes the eightfold symmetry of gp210 proteins around the nuclear pore complex and resolves the central channel with nanometer resolution, J. Cell Sci. 125 (2012) 570–575.
[46] A. Pertsinidis, et al., Subnanometre single-molecule localization, registration and distance measurements, Nature 466 (2010) 647–651.
[47] J. Rauch, et al., Measurement of local chromatin compaction by spectral precision distance microscopy, Proc. SPIE 4164 (2000) 1–9.
[48] L. Rayleigh, On the theory of optical images with special reference to the microscope, Philos. Mag. 5 (1896) 167–195.
[49] J. Reymann, et al., High-precision structural analysis of subnuclear complexes in fixed and live cells via spatially modulated illumination (SMI) microscopy, Chromosom. Res. 16 (2008) 367–382.
[50] M.J. Rust, et al., Sub-diffraction-limit imaging by stochastic optical reconstruction microscopy (STORM), Nat. Methods 3 (2006) 793–795.
[51] S.-H. Shima, et al., Super-resolution fluorescence imaging of organelles in live cells with photoswitchable membrane probes, Proc. Natl. Acad. Sci. U. S. A. 109 (2012) 13978–13983.
[52] H. Shroff, et al., Live-cell photoactivated localization microscopy of nanoscale adhesion dynamics, Nat. Methods 5 (2008) 417–423.
[53] G. Shtengel, et al., Interferometric fluorescent super-resolution microscopy resolves 3D cellular ultrastructure, Proc. Natl. Acad. Sci. U. S. A. 106 (2009) 3125–3130.
[54] J.J. Sieber, et al., Anatomy and dynamics of a supramolecular membrane protein cluster, Science 317 (2007) 1072–1076.
[55] D. Sinnecker, et al., Reversible photobleaching of enhanced green fluorescent proteins, Biochemistry 44 (2005) 7085–7094.
[56] L. Spicuzza, et al., New and emerging infectious diseases, Allergy Asthma Proc. 28 (2007) 28–34.
[57] C. Steinhauer, et al., Super resolution microscopy on the basis of engineered dark states, J. Am. Chem. Soc. 130 (2008) 16840–16841.
[58] D.E. Swayne, et al., in: Y.M. Saif, et al., (Eds.), Influenza in Diseases of Poultry, 5th ed., Blackwell Publishing, Ames, IA, 2008, pp. 153–184.
[59] S. Tamura, et al., Cross-protection against influenza IAV infection afforded by trivalent inactivated vaccines inoculated intranasally with cholera toxin B subunit, J. Immunol. 149 (1992) 981–988.
[60] S. Van de Linde, et al., Direct stochastic optical reconstruction microscopy with standard fluorescent probes, Nat. Protoc. 6 (2011) 991–1009.
[61] A.M. van Oijen, et al., 3-Dimensional super-resolution by spectrally selective imaging, Chem. Phys. Lett. 192 (1998) 182–187.
[62] X. Wang, et al., The interferon-inducible protein viperin inhibits influenza IAV release by perturbing lipid rafts, Cell Host Microbe 2 (2007) 96–105.
[63] K.M. Weidner, et al., The Met receptor tyrosine kinase transduces motility, proliferation, and morphogenic signals of scatter factor/hepatocyte growth factor in epithelial cells, J. Cell Biol. 121 (1993) 145–154.
[64] X. Zhuang, Nano-imaging with STORM, Nat. Photonics 3 (2009) 365–367.
[65] E. Zwick, et al., Receptor tyrosine kinase signalling as a target for cancer intervention strategies, Endocr. Relat. Cancer 8 (2001) 161–173.